https://doi.org/10.5194/egusphere-2022-1108
Preprint. Discussion started: 2 November 2022

Characteristics of Negative Cluster Ions in an Urban Environment

Rujing Yin[1,2#], Xiaoxiao Li[1,3#], Chao Yan[2,4], Runlong Cai[2], Ying Zhou[4], Juha Kangasluoma[2], Nina Sarnela[2], Janne Lampilahti[2], Tuukka Petäjä[2], Veli-Matti Kerminen[2], Federico Bianchi[2], Markku Kulmala[2,4], Jingkun Jiang[1*]

[1]State Key Joint Laboratory of Environment Simulation and Pollution Control, School of Environment, Tsinghua University, Beijing, 100084, China

[2]Institute for Atmospheric and Earth System Research/Physics, Faculty of Science, University of Helsinki, 00014 Helsinki, Finland

[3]School of Resources and Environmental Sciences, Wuhan University, 430072 Wuhan, China

[4]Aerosol and Haze Laboratory, Beijing Advanced Innovation Center for Soft Matter Science and Engineering, Beijing University of Chemical Technology, 100029 Beijing, China

[#]These authors contributed equally to this work.

*: *Correspondence to*: J. Jiang (jiangjk@tsinghua.edu.cn)

This PDF file includes:

Main text

Figures 1 to 7

https://doi.org/10.5194/egusphere-2022-1108
Preprint. Discussion started: 2 November 2022

Abstract. Atmospheric cluster ions are important constituents in the atmosphere. Concentrations and compositions of cluster ions govern their effects on atmospheric chemistry, air quality, and human health. However, quantitative research on ion composition is rare, especially in an urban atmosphere where pollution levels and human populations are intense. In this study, we measure negative cluster ion compositions using an atmospheric pressure interface high-resolution time-of-flight mass spectrometer in urban Beijing. We demonstrate the feasibility of quantifying cluster ion compositions with simultaneous *in-situ* measurements by a neutral cluster and air ion spectrometer. The median concentrations of negative cluster ions smaller than 1.6 nm were 85 (61-112 for 25-75%) cm^{-3}, decreasing significantly with an increasing condensation sink (CS). These concentrations are far lower than those observed at comparatively clean sites due to the higher CS in polluted environments. The ions NO_3^- and HSO_4^-, together with organic ions with the adducts of NO_3^- and HSO_4^-, were the most abundant in urban Beijing, and the organic ions in the atmosphere were similar in composition to those oxygenated organic molecules charged in a chemical ionization mass spectrometer with NO_3^- as the reagent ions. It was shown that the ambient atmosphere is a natural ion-molecular reaction chamber with NO_3^- and HSO_4^- as the main reagent ions. Compared to the clean sites, negative cluster ions in Beijing are composed of more NO_3^- and CHON organic ions due to higher NO_x concentrations and higher fractions of CHON molecules in overall oxygenated organic species. Using dynamic equilibrium equations to examine the fate of HSO_4^- and $C_3H_3O_4^-$ in the atmosphere, we found that their main sources to be the ionization of H_2SO_4 and $C_3H_4O_4$ by NO_3^- and their main loss being the condensational loss onto aerosol particles (73-75%), followed by ion-molecule reaction losses (19%), and ion-ion recombination losses (6-8%).

Keywords: cluster ions, ion composition, urban atmosphere, condensation sink, NO_x

1 Introduction

Atmospheric cluster ions are electrically charged atoms, molecules, and molecular clusters. Their mobility is usually larger than 0.5 $cm^2 \cdot V^{-1} \cdot s^{-1}$ (Horrak et al., 2000). The primary ions, such as N_2^+, O_2^+, NO^+, O^-, and O_2^-, are initially formed via cosmic radiation, gamma radiation, and other near-ground local sources, such as radon decay, lightning, plant emissions, waterfall and seashore generation, combustion, and high-voltage transmission lines emission (Carslaw et al., 2002; Eisele, 1989; Hirsikko et al., 2007; Tammet et al., 2006). Primary ions will subsequently undergo ion-molecule reactions, ion-ion recombination, or deposition onto particles, accompanied by the evolution of their electrical mobility, concentration, and composition (Curtius et al., 2006; Harrison, 2003; Kontkanen et al., 2013; Shuman et al., 2015). Atmospheric ions play important roles in atmospheric chemistry (Bates, 1982; Luts and Salm, 1994), ion-induced nucleation (Charlson et al., 1992; Lee et al., 2003; Lovejoy, 2004), atmosphere conductivity (G. Baumgaertner et al., 2013) and air quality (Jiang et al., 2018; Lee et al., 2004). Moreover, atmospheric negative ions can benefit human health at certain levels of concentration, while their low concentrations may cause headaches and insomnia (Chu et al., 2019; Jiang et al., 2018; Malcolm et al., 2009). The effects of atmospheric cluster ions are highly related to their mobility, concentration and composition (Jiang et al., 2018).

There are substantial differences in the characteristics of atmospheric ions and their dynamic variations among diverse

https://doi.org/10.5194/egusphere-2022-1108
Preprint. Discussion started: 2 November 2022

environments. Globally, atmospheric ion concentrations span a wide range from 100 to 5000 cm^{-3} (Hirsikko et al., 2011; Usoskin et al., 2004), determined mainly by differences in ion production and loss rates. On one hand, ion production rates vary with a geographical location, land cover type and weather conditions (Chen et al., 2016; Ling et al., 2010; Usoskin et al., 2004). On the other hand, ion loss rates are largely related to ions carrying opposite charges, aerosol surface area concentrations, and deposition rates (Harrison, 2003; Tammet et al., 2006). For ion compositions, hundreds of new ions can be formed through ion-molecule reactions after the primary ions are initially formed. It has been found that besides the primary ions, NO_3^-, HSO_4^- and their clusters were predominant ions due to their high acidities (Davidson et al., 1977; Viggiano et al., 1980). Oxygenated organic molecules (OOMs) were observed clustering with NO_3^- and HSO_4^- naturally in the atmosphere and the composition of these organic atmospheric ions has been reported to be similar to those of neutral vapor molecules (Bianchi et al., 2017; Ehn et al., 2010; Yin et al., 2021). Specifically, ion compositions were found very different between NPF and non-NPF events, and ion compositions during NPF implies different nucleation pathways in clean and polluted atmospheres (Bianchi et al., 2016; Ehn et al., 2010; Eisele et al., 2006; Kirkby et al., 2016; Yin et al., 2021). Thus, the measurement of ion characteristics requires high temporal measurements in various environments.

Ion characteristics at polluted urban sites, where the ion production and loss processes may be very different from the clean sites, are relatively poorly understood. At many polluted urban sites, intense pollution emissions lead to high concentrations of neutral gas species and high aerosol concentrations. For the ion production processes, the neutral gas molecules at the urban site are significantly different from those at clean sites. High NO_x concentrations were found to be accompanied with high concentrations of nitrogen-containing organic molecules at polluted urban sites (Li et al., 2022; Qiao et al., 2021). For ion loss processes, condensation sink (CS) at urban sites can reach up to two orders of magnitude higher values compared with clean sites (Cai et al., 2017), which would cause a significant loss of ions onto large particles in urban air. These may lead to big differences in ion concentrations and compositions between clean and urban sites. For instance, Iida et al. (2006) have shown that the ion concentration near a polluted site Boulder might be substantially suppressed by high ion loss rates, resulting only a minor contribution from ion-induced nucleation to NPF. Although some recent studies have revealed the characteristics of ions in clean environments (Bianchi et al., 2016; Chen et al., 2016; Ehn et al., 2010), only few studies have focused on such characteristics in an urban atmosphere (Yin et al., 2021).

Simultaneous analysis of ion concentrations and compositions are rare in the field campaign. Various ion counters have been designed to measure ion concentrations in the last century. Among these, Gerdien counters (Gerdien and H., 1903; Gerdien, 1905), a balance scanning mobility analyzer (BSMA) (Tammet, 2006), the air ion spectrometer (AIS) (Mirme et al., 2007), and a neutral cluster and air ion spectrometer (NAIS) (Manninen et al., 2016; Manninen et al., 2009) are the most widely used ion counters or ion mobility spectrometers. However, these electrical mobility-based instruments do not provide detailed information on an ion composition. Mass spectrometers have been widely used in the measurement of ion compositions. Quadrupole mass spectrometers with approximate integer mass resolution have been applied in a series of ion composition measurements (Eisele, 1989; Eisele et al., 2006; Eisele and Tanner, 1990; Viggiano, 1993). With the development of high-resolution mass spectrometer techniques, such as an atmospheric pressure interface time-of-flight mass spectrometer (APi-TOF, Tofwerk AG), more species of atmospheric ions were identified (Ehn et al.,

https://doi.org/10.5194/egusphere-2022-1108
Preprint. Discussion started: 2 November 2022

2010; Eisele et al., 2006; Junninen et al., 2010; Kirkby et al., 2016), but the quantification of those ions in the APi-TOF remains to be addressed.

It is urgent to develop a robust and easy-to-use method to quantify concentrations of different ions in APi-TOF in field measurements. The detection efficiency of an APi-TOF to different ions is mainly determined by the *m/z*-dependent transmission efficiency. The calibration of transmission efficiency often requires complex laboratory calibration settings, including the generation, classification and counting of ions with different *m/z* ratios (Heinritzi et al., 2016; Junninen et al., 2010). Alternatively, the relative transmission efficiency of an APi-TOF compared to primary ions can be obtained using a depletion method with the help of a chemical ionization inlet (Heinritzi et al., 2016). But the settings are still complex and only relative transmission efficiency is obtained. For convenience, an *in-situ* calibration method was proposed by Ehn et al. (2011), in which the measured results of a NAIS and APi-TOF in Hyytiälä showed good correlations for size-segregated ions. Since ion mobility was negatively correlated with the *m/z* of the ions (Horrak et al., 2000), it is possible to calibrate the mass spectrometers *in-situ* using the synchronous measurements of well-calibrated ion spectrometers (e.g. NAIS). However, the feasibility of this method in polluted urban atmospheres still needs to be examined.

In this study, we apply an *in-situ* quantification method of atmospheric ion compositions measured by an APi-TOF and reveal the governing factors of atmospheric cluster ion concentration and composition at polluted urban sites. We perform field measurements of atmospheric negative cluster ions at an urban site using the APi-TOF and NAIS simultaneously. By comparing the two *in-situ* measurements, we quantify the concentration of ions measured by the APi-TOF using an improved method. The concentration and composition of ions are compared with the clean sites, and the reasons for the observed differences are explored. The origins and composition variations of ions are characterized and compared with the neutral clusters measured by a chemical ionization mass spectrometer with NO_3^- as the reagent ions (abbreviated as (nitrate) CI-APi-TOF). The driving factors for the variations in ion characteristics at the urban site are revealed. To better quantify the formation and loss scheme of atmospheric ions, the ions HSO_4^- and $C_3H_3O_4^-$ are taken as representatives in the dynamic equilibrium equation. We further show that ion concentrations can be well-predicted by neutral molecule concentration and CS using H_2SO_4 and $C_3H_4O_4$ as examples

2 Methods

2.1 Field measurement

A field measurement is conducted at the Aerosol and Haze Laboratory of Beijing University of Chemical Technology Station (AHL/BUCT station), Beijing, China (Liu et al., 2020; Yin et al., 2021). The AHL/BUCT station is a typical urban site surrounded by three traffic roads and some residential buildings. The station is ~18 m above the ground with no higher buildings around it within 50 m. It is equipped with many state-of-the-art instruments and routine instruments for air quality measurements. This station has been continuously operated since 2018. The sampling period used in this study is between Jan 14th and Sep 16th, 2018. Besides the measurement in urban Beijing, the measurement at a boreal forest site (Hyytiälä) during 2013 is used for comparison (Manninen et al., 2009; Yan et al., 2018).

https://doi.org/10.5194/egusphere-2022-1108
Preprint. Discussion started: 2 November 2022

The atmospheric negative cluster ion compositions were measured with an atmospheric pressure interface time-of-flight high-resolution mass spectrometer (APi-HTOF) from Feb 14th to Feb 27th, 2018. The ambient air is sampled from the window through a 1.4-m long 1/4 in, stainless steel tubing. The sampling flow rate of the APi-HTOF is ~0.8 LPM, and the extra sheath flow is 3 LPM, resulting in a total sampling flow rate of 3.8 LPM. The APi-HTOF was operated in a negative ion mode to measure negative ions, and the voltages in the APi-HTOF were adjusted to minimize cluster fragmentations. As atmospheric ion concentrations are relatively low, signals were averaged to 1 h for further analysis. The mass resolution of the APi-HTOF is ~4500 at *m/z* 200. The elements C, H, O, N, and S were used for peak assignment. Peaks that cannot be assigned with these elements within 10 ppm are labeled as "unknown" or "others". The relative mass-dependent transmission efficiency in the HTOF was calibrated through the depletion method when the APi-HTOF was operated with a nitrate chemical ionization (CI) inlet in front, for which the voltages were kept the same as in the APi-mode (Heinritzi et al., 2016). Detailed descriptions of the measurement and data analysis have been described in our previous study (Yin et al., 2021).

The neutral gas molecules were measured by a (nitrate-) CI-APi-LTOF (Bertram et al., 2011; Jokinen et al., 2012), where NO_3^- and its adducts $(HNO_3)_{1-2}NO_3^-$ are used as the reagent ions to chemically ionize the gas molecules with a laminar flow ionization source mounted in front of the APi-LTOF (Eisele and Tanner, 1993). The species that can be ionized by NO_3^- and its adducts $(HNO_3)_{1-2}NO_3^-$ are usually highly oxygenated molecules, such as H_2SO_4 and OOMs. The mass resolution is ~8000 at *m/z* 200. The peak fitting and identification of the molecular compositions use binPMF solutions as an assistant for the complex mass spectra following our previous studies (Nie et al., 2022) . For quantification, we performed H_2SO_4 sensitivity calibration via the controlled reaction between SO_2 and OH (Kürten et al., 2012; Li et al., 2019). The relative mass-dependent transmission efficiency of the CI-APi-LTOF was also calibrated through the depletion method (Heinritzi et al., 2016), and these results are shown in our previous study (Yin et al., 2021).

The ion mobility distribution was measured by a NAIS (NAIS, Airel Ltd.) (Mirme and Mirme, 2013). It can simultaneously measure positive and negative ions with ion mobility of 3.2-0.0013 $cm^2 \cdot V^{-1} \cdot s^{-1}$, corresponding to the mobility diameter range of 0.8-40 nm. In practice, the NAIS switched between detecting naturally charged ions and total particles (including neutral and charged particles) by switching off/on a unipolar corona charger. The measurement cycle period was 2 min for the ion mode, 2 min for the particle mode, and 30 s for offset. As we focus on atmospheric ions, the data measured in particle mode was not used in our following analysis. For the ion measurement, two cylindrical mobility spectrometers were operated in parallel to measure positive and negative ions simultaneously. An overall of 109 mobility bins are divided. In this study, only negative ions with mobility diameters smaller than 1.6 nm were used, corresponding to ion mobility of ~0.8 $cm^2 \cdot V^{-1} \cdot s^{-1}$, as we only focus on cluster ions. The results of NAIS were calibrated considering both the transfer functions and sampling losses.

2.2 The quantification of air ions

Although we calibrated the relative *m/z*-dependent transmission efficiency in the APi-HTOF, there are still two problems for accurate quantification: (1) the absolute transmission efficiency is unknown and needs to be calibrated; (2) the relative transmission efficiency curve is calibrated by adding a CI-inlet in front of the APi-HTOF, and the influences of CI-inlet remain unknown. For example, a previous study using a high-resolution differential mobility analyzers and electrometer

https://doi.org/10.5194/egusphere-2022-1108
Preprint. Discussion started: 2 November 2022

to calibrate the transmission efficiencies under the APi-mode and CI-mode found that the transmission efficiency under the CI-mode shifts to larger *m/z* compared to APi-mode (Heinritzi et al., 2016).

Considering these two problems in quantifying APi-HTOF, we used an improved method to obtain the absolute transmission efficiency of the APi-HTOF through the comparison with the synchronous *in-situ* measurement from the NAIS. The key to linking the measurement results of ions by the APi-HTOF with those by the NAIS is to convert the *m/z* of ions to ion mobilities. As the resolving power of the NAIS is lower than that of the APi-HTOF, the ion signals in APi-HTOF in specific *m/z* ranges were summed up to compare with the ion concentrations measured by the NAIS.

For some specific ions with known peak assignments and structures, like NO_3^- and HSO_4^-, the ion mobility can be directly measured by ion mobility spectrometers (IMS). The results reported in previous literature (Jen et al., 2015; Liang et al., 2013; Spangler and Collins, 1975; Stano et al., 2008) are summarized in Table S1 and were applied in this study. For the remaining ions, like the hundreds of complex organic ions, the Stokes-Millikan equation was applied to convert their *m/z* to mobilities (Ehn et al., 2011; Friedlander, 2000; Tammet, 1995), as in Eq. 1.

$$Z = \frac{1}{\sqrt{1+m_g/m}} \frac{Q}{3\pi\mu} \frac{1+Kn\left(1.257+0.4e^{-1.1/Kn}\right)}{d_m+d_g} \quad \text{Eq.1}$$

where Z is the electrical mobility, m_g the mass of a carrier gas molecule, m the mass of ions, Q the charge of ions, μ the viscosity of the carrier gas, Kn the Knudsen number, d_m the mobility diameter of ions, and d_g the diameter of the carrier gas molecule. Here, the carrier gas is ambient air, and m_g, d_g, and μ are adopted as 29.0 g/mol, 0.3 nm, and 1.73×10^{-5} $kg\cdot m^{-1}\cdot s^{-1}$ at 278 K and 101.3 kPa (Ku and De La Mora, 2009). Kn and d_m are calculated as Eq. 2-3.

$$K_n = \frac{2\lambda}{d_m+d_g} \quad \text{Eq.2}$$

$$d_m = \sqrt[3]{\frac{6m}{\pi\rho}} \quad \text{Eq.3}$$

where λ is the mean free path of carrier gas (62 nm at 278 K and 101.3 kPa) and ρ the density of ions. The appropriate density for calculating the mobility of ions is controversial. Ehn et al. (2011) used the bulk density of aconitic acid (1.66 $g\cdot cm^{-3}$) for the conversion, but molecular clusters may have different densities with bulk substances. To investigate this problem, we compared the measured mobility of an IMS for different types of OOMs with the calculated mobilities according to the Stokes-Millikan method using 1.1, 1.3, and 1.6 $g\cdot cm^{-3}$ as the densities respectively (Fig. S1). The experimental results of the IMS are from Krechmer et al. (2016). By comparing the measured and calculated mobilities for organic ions with different compositions, densities of 1.1 and 1.3 $g\cdot cm^{-3}$ were ultimately used in the mass-mobility conversion of ions with *m/z* smaller and larger than 150, respectively. The sudden change of density at *m/z* 150 led to an increase in estimated mobility from 1.67 to 1.80, which should have had limited influences on the final calibration results. Finally, the mobilities of all ions were adjusted according to the ambient temperature and pressure before being applied in the calibration of APi-HTOF (Tammet, 1995).

Using the synchronous *in-situ* measurement results of the NAIS as the reference, the detection efficiency of the APi-HTOF for ions with different *m/z* is obtained. Here, since the ion concentrations measured by the NAIS have already considered sampling losses and represent atmospheric concentrations, the obtained detection efficiency of the APi-HTOF

https://doi.org/10.5194/egusphere-2022-1108
Preprint. Discussion started: 2 November 2022

should represent a combined result of the transmission efficiency of the APi-HTOF and the sampling efficiency in the sampling line of the APi-HTOF. The ions used in the APi-HTOF are in the *m/z* range from 32 to 908, corresponding to the mobility diameters of 0.8-1.6 nm and ion mobilities of 3.16 to 0.77 $cm^2 \cdot V^{-1} \cdot s^{-1}$, covering 12 mobility bins of the NAIS measurements. The number concentrations and signal intensities measured by the NAIS and APi-HTOF had good consistencies ($r \geq 0.66$) in the 12 bins, and the correlations were the best over the *m/z* range of 331-791 ($r > 0.94$) (Fig. S2). The good correlation between the APi-HTOF and NAIS indicates that both instruments captured the variation of the atmospheric negative cluster ions. Then the detection efficiency of a certain *m/z* in the APi-HTOF was calculated as the slope of the linear fitting line between signal intensities acquired in the APi-HTOF and number concentrations in the NAIS. Comparing with the detection efficiencies calculated from the composition-dependent density, using a fixed density of 1.66 $g \cdot cm^{-3}$ would overestimate the detection efficiency for small ions and underestimate that for large ions, with a deviation of up to 40% (Fig. S3).

After excluding the effect of sampling losses in the APi-HTOF, the absolute transmission efficiency of the APi-HTOF was derived, and the obtained pattern agreed well with the relative transmission efficiency as shown in Fig. 1. As the composition-dependent density was applied, the absolute and relative transmission efficiency curves showed similar patterns with both peaking at ~*m/z* 400, where the absolute transmission efficiency reached ~4.9%. The discrepancy between the absolute and relative transmission efficiency at small values of m/z may be caused by the uncertainty of small ion measurements in the NAIS, sampling efficiency calculation, or the influences of CI-inlet, as the voltage settings remain the same during the calibration experiment. The absolute transmission efficiency obtained by our calibration is roughly the same order of magnitude as that in previous studies, and the shape is similar as well (Heinritzi et al., 2016; Junninen et al., 2010). Finally, the fit line of the detection efficiency was applied to quantify the ion compositions measured by the APi-HTOF, considering both the sampling efficiency and the transmission efficiency (Fig. 1).

Fig. 1 The detection and transmission efficiency curves

The total negative cluster ion concentrations measured by the APi-HTOF were well consistent with those measured by the NAIS (Fig. 2). However, when the total ion concentrations were smaller than ~70 cm^{-3}, the total ion concentrations measured by the NAIS were higher than those measured by the APi-HTOF. Specifically, total cluster ion concentration measured by the NAIS was still higher than 25 cm^{-3} even when ions detected by APi-HTOF approached zero. These signals detected by the NAIS are mainly from small cluster ions (3.16-1.28 $cm^2 \cdot V^{-1} \cdot s^{-1}$, 0.8~1.27 nm), the fraction of which rises to >80% of the total counts when the total cluster ion concentration measured by the APi-HTOF is lower than ~70 cm^{-3}. As the APi-HTOF has a much lower detection limit than the NAIS (Fig. S4), these signals could be caused by the high noise of small ions in the NAIS. The detection limit of the APi-HTOF is determined according to the noise of microchannel plate (MCP) detector and the detection efficiency. The detection limit of the APi-HTOF is the lowest at a diameter of 1.4 nm, which is ~0.02 cm^{-3}, and it increases when the detected ions move to lower or higher sizes due to the decrease in detection efficiency. The detection limit of the NAIS is determined according to the noise of the electrometer and its transfer function, and the noise of the electrometer was assumed to be 0.006 fA in our study. The detection limit of the NAIS decreases with an increasing in ion diameter. The detection limit of the NAIS for cluster ions is within 30-300 cm^{-3}. Thus, the ion concentration measured by the APi-HTOF is more reliable than that measured by

https://doi.org/10.5194/egusphere-2022-1108
Preprint. Discussion started: 2 November 2022

the NAIS when the ion concentration is extremely low. As the influence of background noise would diminish when signals increase and the detection efficiency is calculated using data during the whole period, the background noise in the NAIS has limited influence on the calibration we have done above.

Fig. 2 Ion concentrations measured by APi-HTOF and NAIS

2.3 The simulation of HSO_4^- and $C_3H_3O_4^-$ concentration

To quantitatively address the sources and sinks of air ions, we simulate the concentration of ions through the dynamic equilibrium equation and identify their dominant production and loss pathways. The simulated concentrations are compared with the measured concentrations. The ions HSO_4^- and $C_3H_3O_4^-$ are chosen here, as their concentrations are relatively high in urban Beijing and their reaction constants are relatively well known. The production pathways considered in this simulation are the ion-molecular reactions between NO_3^- and neutral molecules H_2SO_4 and $C_3H_4O_4$. Previously, NO_3^- has been found to be formed earlier during the evolution of ion clusters (Beig and Brasseur, 2000; Luts, 1995) and to ionize neutral gaseous that are more acidic than HNO_3, such as H_2SO_4 and $C_3H_4O_4$ (Eisele, 1989; Tanner and Eisele, 1991). The loss pathways in the atmosphere mainly include the condensational loss onto the particles, ion-molecules reactions, and ion-ion recombination between ions of opposite charge. The formation of H_2SO_4 dimer ions could be an important loss pathway for HSO_4^- (Beck et al., 2022). $C_3H_3O_4^-$ could further react with H_2SO_4 and change back to the neutral form $C_3H_4O_4$ (Beig and Brasseur, 2000). Thus, the following ion-molecule reactions are considered in the dynamic models to simulate the formation of HSO_4^- and $C_3H_3O_4^-$ in urban Beijing.

$$NO_3^- + H_2SO_4 \xrightarrow{k_1} HSO_4^- + HNO_3 \quad \text{R.1}$$

$$NO_3^- + C_3H_4O_4 \xrightarrow{k_2} C_3H_3O_4^- + HNO_3 \quad \text{R.2}$$

$$C_3H_3O_4^- + H_2SO_4 \xrightarrow{k_3} HSO_4^- + C_3H_4O_4 \quad \text{R.3}$$

$$HSO_4^- + H_2SO_4 \xrightarrow{k_4} H_2SO_4 \cdot HSO_4^- \quad \text{R.4}$$

where k_1 to k_4 are the rate constants of these reactions, which are 2.32×10^{-9}, 2.5×10^{-9}, 2.0×10^{-9}, and 2.0×10^{-9} $cm^3 \cdot s^{-1}$ respectively (Beig and Brasseur, 2000; Lovejoy and Curtius, 2001; Viggiano et al., 1997).

The dynamic equilibrium equations for HSO_4^- and $C_3H_3O_4^-$ can be written as Eq.4 and Eq.5, respectively.

$$\frac{d[HSO_4^-]}{dt} = k_1[NO_3^-][H_2SO_4] - k_4[HSO_4^-][H_2SO_4] - CS[HSO_4^-] - \alpha n^+[HSO_4^-] \quad \text{Eq.4}$$

$$\frac{d[C_3H_3O_4^-]}{dt} = k_2[NO_3^-][C_3H_4O_4] - k_3[C_3H_3O_4^-][H_2SO_4] - CS[C_3H_3O_4^-] - \alpha n^+[C_3H_3O_4^-] \quad \text{Eq.5}$$

where $CS[HSO_4^-]$ and $CS[C_3H_3O_4^-]$ are loss rates caused by the condensational loss onto particles; $\alpha n^+[HSO_4^-]$ and $\alpha c^+[C_3H_3O_4^-]$ are loss rates caused by the ion-ion recombination between ions of opposite charge; the value of α is assumed to be 1.6×10^{-6} $cm^3 \cdot s^{-1}$ (Bates, 1982; Zauner-Wieczorek et al., 2022); n^+ is the total concentration of positive ions and is measured by NAIS. Thus, the concentration of HSO_4^- and $C_3H_3O_4^-$ are calculated as in Eq.6 and Eq.7,

https://doi.org/10.5194/egusphere-2022-1108
Preprint. Discussion started: 2 November 2022

respectively. Note that the HSO_4^- formed through the ion-molecule reaction between $C_3H_3O_4^-$ and H_2SO_4 is neglected considering the low concentration of $C_3H_3O_4^-$ in Beijing.

$$[HSO_4^-] = \frac{k_1[NO_3^-][H_2SO_4]}{CS + k_3[H_2SO_4] + \alpha n^+} \quad \text{Eq.6}$$

$$[C_3H_3O_4^-] = \frac{k_5[NO_3^-][C_3H_4O_4]}{CS + k_2[H_2SO_4] + \alpha n^+} \quad \text{Eq.7}$$

3. Results and discussion

3.1 Ion concentrations

The median concentration of negative cluster ions was 85 cm^{-3} in Beijing during the measurement period, and its 25th and 75th percentiles were 61 cm^{-3} and 112 cm^{-3} respectively. These values were significantly lower than concentrations typically reported at rural, forest and marine sites (Fig. 3a). The total concentration of air ions ranged between 14 cm^{-3} and 467 cm^{-3} in urban Beijing, similar to that in the Indian urban city, Pune, which is also a highly polluted site (Gautam et al., 2017). Ion concentrations in these two polluted urban cities are so far the lowest, significantly lower than at other urban, rural and marine or forest sites, which are mostly above 200 cm^{-3} (Chen et al., 2017; Dos Santos et al., 2015; Hirsikko et al., 2011; Tammet, 2015a; Tammet, 2015b). It should be noted that although Paris is an urban site, its air is relatively clean in terms of aerosol concentration compared to the Chinese and Indian polluted urban sites. Similarly, cluster ion concentrations at some urban sites can also be as high as those at rural and remote sites due to the relatively clean atmosphere (Hirsikko et al., 2011).

Fig. 3 Concentration comparison between Beijing and other sites.

The ion concentrations are negatively correlated with CS at both urban Beijing and the clean forest site Hyytiälä. In urban Beijing, the median ion concentration decreases from 181 to 51 ions cm^{-3} when CS increases from 0.0032 to 0.12 s^{-1} (Fig. 3b). The negative correlation between the ion concentration and CS exists for all the mobility ranges and is more intensive for ions with an electrical mobility between 1.72 and 0.90 $cm^2 \cdot V^{-1} \cdot s^{-1}$, corresponding to a diameter range of about 1.03-1.44 nm (Fig. S5). Such negative correlation is also observed in Hyytiälä, where the median ion concentrations decrease from a median of 606 to 369 ions cm^{-3} when CS increases from 0.00017 to 0.012 s^{-1}. Combining data from these two sites, a negative correlation can still be seen over a wide CS range of 0.00017 to 0.12 s^{-1}. The influence of CS on the positive cluster ions also exists, as positive and negative ions are closely related to each other (Fig. S6). Thus, CS is an important influencing factor for the total cluster ion concentrations in both Beijing and Hyytiälä. This is very likely the reason for the lowest ion concentrations at the two polluted sites (Beijing and Pune, Fig. 3a) having the highest aerosol mass loadings. Overall, the inverse relation between the negative cluster ion concentration and CS was much stronger in Beijing compared with Hyytiälä (Fig. 3b).

https://doi.org/10.5194/egusphere-2022-1108
Preprint. Discussion started: 2 November 2022

In urban Beijing, the estimated lifetime of cluster ions due to the combined effect of condensation loss and ion-ion recombination of cluster ions is 0.02-0.4 min during haze periods ($PM_{2.5}$ > 75 μg/m^3, average CS = 0.091 s^{-1}) and 0.1-1.6 min during clean periods ($PM_{2.5}$ < 75 μg/m^3, average CS=0.023 s^{-1}) (Fig. S7). The lifetime of cluster ions in Hyytiälä is between 0.8-14 min (average CS = 0.0018 s^{-1}), much longer than that in Beijing. Such distinct CS reliance in urban Beijing is barely observed in previous studies despite the condensational loss of ions on large particles has been widely recognized as important. On the contrary, most of the studies have found weather conditions and ionizing radiation as the controlling factor for ion concentrations. For example, ion production rates in Hyytiälä were reported to be largely affected by variations in seasonal radiation and wind speed (Chen et al., 2016). This indicates that CS may be the driving factor of cluster ion concentration only at highly polluted sites with high aerosol mass loadings and relatively constant ion production rates, while ion production rates may be the driven factor at relatively clean sites where aerosol mass loadings are low and ion production rate varies significantly (Hirsikko et al., 2007).

3.2 Ion compositions

Inorganic nitrogen-containing ions, inorganic sulfur-containing ions and organic ions were found to be the most abundant negative ions in urban Beijing, representing 20-22%, 8-15%, and 37-43% of the total negative cluster ion concentrations (Fig. 4a). Inorganic nitrogen-containing ions were mainly detected as NO_2^-, NO_3^-, and $HNO_3NO_3^-$, possibly existing in the forms of $NO_2^-\cdot(H_2O)_n$, $NO_3^-\cdot(H_2O)_n$, and $NO_3^-\cdot HNO_3\cdot(H_2O)_n$ in the atmosphere (Luts, 1995), with the loosely bounded water molecules being evaporated from the cluster ions when passing through the mass spectrometer. The concentration of NO_2^- and NO_3^- were observed to be well correlated with each other in the atmosphere of Beijing, and the concentration of NO_2^- was ~20 % of that of NO_3^- (Fig. S8a). This is consistent with the ion chemical models suggesting that NO_2^- and NO_3^- can be stably formed through a series of reactions between primary ions, NO, NO_2, and HNO_3 in the atmosphere (Beig and Brasseur, 2000; Kawamoto and Ogawa, 1984). $HNO_3NO_3^-$ is subsequently formed by adding an HNO_3 molecule to NO_3^-. Inorganic sulfur-containing ions are mainly in the form of HSO_4^-, SO_5^-, and $H_2SO_4HSO_4^-$. The ion HSO_4^- is mainly produced by the ion-molecule reaction between NO_3^- and H_2SO_4 which will be discussed hereinafter. $H_2SO_4HSO_4^-$ is formed by the further addition of an H_2SO_4 molecule, which is proposed as the first step of ion-induced nucleation (Lovejoy, 2004). SO_5^- is likely to be generated through the reaction between O_2 and SO_3^- (Möhler et al., 1992), and its signal variation was similar to that of HSO_4^- (Fig. S8b). Similar compositions and variations of inorganic sulfur-containing ions have been observed at a clean site (Ehn et al., 2010). The organic ions were mainly CHON organic or CHO organic ions. They were mainly in the form of the adduct with NO_3^- or HSO_4^-, with minor fractions in the deprotonated form CHO^-, indicating that the ionization schematic of these organic ions is mainly through ion-molecular reaction with NO_3^- or HSO_4^-. Some sulfur-containing organics may be distinguished as CHON-HSO_4^- ions, but as few neutral gases have been observed with sulfur, it is unlikely that CHON-HSO_4^- is a cluster of organic sulfate (CHOS) and NO_3^- ions (Bianchi et al., 2017; Ehn et al., 2010).

Fig. 4 Composition comparison between Beijing and Hyytiälä

https://doi.org/10.5194/egusphere-2022-1108
Preprint. Discussion started: 2 November 2022

Ion compositions during clean and haze periods in urban Beijing were very different (Fig. 4b), influenced mainly by the differences in neutral gaseous molecules. During the haze periods, the organic ions were dominated by nitrated phenol compounds, such as $C_6H_5NO_3 \cdot NO_3^-$ and $(C_6H_5NO_3)_2 \cdot NO_3^-$. The high nitrated phenol ions in the haze periods are the result of high anthropogenic emissions of aromatics and high NO_x concentrations (30.1±14.6 ppb) (Cheng et al., 2021). During the clean periods when the average NO_x decreased to 15.0±11.5 ppb, a series of organic ion peaks were observed for *m/z* above 300. The highest peaks in the series include $C_{10}H_{15}NO_{10} \cdot NO_3^-$, $C_{10}H_{14}O_{11} \cdot NO_3^-$, and $C_{10}H_{16}NO_{11} \cdot NO_3^-$, which are possibly the ionization form of highly oxygenated products from monoterpenes (Lehtipalo et al., 2018). Also the ions HSO_4^- and $H_2SO_4HSO_4^-$ were more abundant during the clean periods, indicating that the ion-induced nucleation is stronger under clean conditions than during haze periods in Beijing due to the low CS.

Compared with the clean forest site Hyytiälä, higher fractions of NO_3^- and nitrogen-containing organic ions were observed in urban Beijing, especially during the haze periods, which can be attributed to the high NO_x concentrations (Fig. 4a-b). Firstly, the inorganic ions, including nitrogen- and sulfur-containing ions, were more abundant in Beijing (37-42%) than in Hyytiälä (10%). This is due to the high concentrations of nitrogen- and sulfur-containing neutral gases, including NO_x, SO_2, HNO_3, H_2SO_4. Secondly, CHON fractions (24-32%) were much higher than CHO fractions (9-11%) in urban Beijing, whereas the CHO organic ions (46%) were more abundant than the CHON fractions (31%) in Hyytiälä. This is consistent with previous studies showing that neutral OOMs are composed of more nitrogen-containing species in urban Beijing compared with Hyytiälä due to the high NO_x concentration (Li et al., 2022; Qiao et al., 2021). Thirdly, nearly all the organic ions were in the form of adducts with NO_3^- in Hyytiälä, whereas some fraction of the organic ions was adducted with HSO_4^- in Beijing. This is related to the higher HSO_4^-/NO_3^- ratio in Beijing (~0.3) compared with Hyytiälä (~0.1). The smaller fraction of organic-HSO_4^- ions in Hyytiälä has also been observed in previous studies (Bianchi et al., 2017; Yan et al., 2018). Finally, the spectrum during the clean periods in Beijing had more similarities to the ion spectrum in Hyytiälä. The latter site is known to be dominated by biogenic volatile organic compounds such as monoterpenes (Isidorov et al., 1985), so the corresponding ion spectrum is dominated by monoterpene-related OOMs. In summary, the observed composition differences were mainly caused by the high NO_x in urban Beijing. Despite the compositions in urban Beijing and forest Hyytiälä being different, the ion mobility distributions were generally quite similar (Fig. 4c). The mode mobility peaks of ions for both sites were ~2 $cm^2 \cdot V^{-1} \cdot s^{-1}$, corresponding to the *m/z* range of 118-239 dominated by HSO_4^- dimer, trimer, and organic ions.

3.3 Comparison of ion and neutral molecules

In the above analysis, we showed that the detected negative organic ions are mostly in the form of the adduct with NO_3^- and HSO_4^-. We thus compared the organic ion composition with the spectra measured with a (nitrate-) CI-APi-LTOF. The organic ions measured by the APi-HTOF were similar to the ionized organic molecules in the (nitrate) CI-APi-LTOF. There was a total of 253 ions measured in both spectra (Fig. 5a). The common ions included $(H_2SO_4)_{0\text{-}3}HSO_4^-$, $(HNO_3)_{0\text{-}2}NO_3^-$, CHO^-, $CHO \cdot NO_3^-$, and $CHON \cdot NO_3^-$ peaks. Such abundant common ions in APi-HTOF and CI-APi-LTOF

https://doi.org/10.5194/egusphere-2022-1108
Preprint. Discussion started: 2 November 2022

indicate their similarities in ionization pathways. The ions detected only by the APi-HTOF were mainly $CHO{\cdot}HSO_4^-$ and $CHON{\cdot}HSO_4^-$ due to the lack of HSO_4^- reagent ions in the CI-APi-LTOF. Also some new particle formation-related large $(H_2SO_4)_m(amine)_n(NH_3)_zHSO_4^-$ clusters (m=1-5, n=0-4, z=0-2) were only detected by the APi-HTOF due to their fragmentation during the chemical ionization process and low signal-to-noise in the CI-APi-LTOF (Yin et al., 2021). Most of the ions detected only by the CI-APi-LTOF were relatively less abundant ions, thus their corresponding ion concentrations were too low to be detected or to be assigned with a certain formula in the APi-HTOF.

Most of the observed negative organic cluster ions in urban Beijing were the result of NO_3^- clustering with OOMs. The presence of these $OOM{\cdot}NO_3^-$ clusters confirms that most of the negative air cluster ions are naturally charged by NO_3^- and neutral OOMs are the preference in this ionization process. The carbon (C) and oxygen (O) element numbers of CHO and CHON species detected in the APi-HTOF and CI-APi-LTOF had similar distributions (Fig. 5b), with C atom in the range of 1 to 14, O atom in the range of 1 to 15, and N atom in the range of 0 to 2 (Fig. S9). The average O:C ratio of the organic ions detected in the APi-HTOF and CI-APi-LTOF were 0.74 and 0.94, respectively. The O:C ratios were significantly higher than those detected by the (iodide)CI-APi-TOF and (oxygen)CI-APi-TOF (Li et al., 2021; Riva et al., 2019), as NO_3^- are more selective towards oxygenated organics than I^- and O_2^-. For a specific CHO molecule, the ratio of its form in $CHO{\cdot}NO_3^-$ to CHO^- were 1.6 and 2.7 on average in APi-HTOF and CI-APi-LTOF, respectively. The lower ratio in the APi-HTOF may be related to the less abundant NO_3^- among the natural ions, as compared with that in the CI inlet. This low ratio could also be introduced by the existence of other reagent ions besides NO_3^-, such as HSO_4^- and O_2^- in the ambient air.

Besides NO_3^-, HSO_4^- is another major reagent ion in the atmosphere. Total organic ion cluster concentrations with the adduct of NO_3^- and HSO_4^- were 27-34% and 7-8%, respectively (Fig. 4a). Natural charge fractions of ions were calculated by comparing the common species measured by the APi-HTOF and CI-APi-LTOF. Fig. 5c shows that the natural charge fractions for these molecules are highly dependent on the chemical compositions and CS. For $CHO{\cdot}HSO_4^-$ and $CHON{\cdot}HSO_4^-$ measured by the APi-HTOF, neutral molecules detected by the CI-APi-LTOF containing the same formula of CHO and CHON are treated as their corresponding precursors. The charge fraction varied greatly between 10^{-10} and 10^{-5}, with highest charge fractions observed for H_2SO_4 (10^{-7}-10^{-5}). The average charge fractions of the organic ions were much lower (10^{-10}-10^{-6}). For example, the charge fraction for $C_3H_4O_4$ was 2×10^{-7}-2×10^{-6}. The charge fraction of CHO was about one order of magnitude higher than that of CHON, regardless of the charge carrier (NO_3^- or HSO_4^-). These values tend to be much lower than the predicted charge fraction of 1 nm particles after a bipolar diffusion charging process (~10^{-3}) (Wiedensohler et al., 1986). Moreover, the ratio of ions formed via a neutral organic compound charged by HSO_4^- and the same compound charged by NO_3^- varied in the range of 0.008-8, with an average of ~0.7 (Fig. S10). The containing of nitrogen atoms in the formula of neutral molecules seemed to have only little influence on this ratio. Besides, we found that the natural charge fractions decreased by 1-2 orders of magnitudes with the increase of CS in urban Beijing. It should be noted that the charge fraction calculation assumes that the CI-APi-LTOF perfectly quantifies

https://doi.org/10.5194/egusphere-2022-1108
Preprint. Discussion started: 2 November 2022

all the species, including the assumption that the ionization efficiency of ions in the CI-APi-LTOF is the same as that of H_2SO_4. It is known that the neutral molecule concentration estimated under this assumption is at the lower limit (Hyttinen et al., 2016), and thus, the calculated charge fractions are most likely at the higher limit.

Fig. 5 Composition comparison between neutral molecules and ions

To sum up, the concentration of a specific ion is determined by the CS, neutral gaseous molecule concentration and reagent ion concentration. As shown in Fig. S11, the concentration of a specific ion was negatively correlated with CS, and under similar CS levels the concentration of ions generally increased with its corresponding neutral gas concentration. The influences of neutral gas and reagent ion concentrations were also reflected in the diurnal variations of HSO_4^-, CHO-related ions and CHON-related ions, as shown in Fig. 6, possibly because the diurnal variations of CS were relatively small compared to the variations in precursor concentrations. It should be noted that nitrated phenol-related ions were not counted as $CHON{\cdot}NO_3^-$ or $CHON{\cdot}HSO_4^-$ here, because nitrated phenol compounds have remarkably high signals and different characteristics, e.g., high volatilities, from most CHON compounds measured in the CI-APi-TOF.

The diurnal variations of ions were mainly determined by their neutral gas molecules, with slight influences from the variations in reagent ions. Among these, HSO_4^- and its neutral molecule H_2SO_4 had the most similar diurnal variations, with distinct peaks at noon and the lowest values at night. The diurnal variations of CHO-related and CHON-related ions also showed some similarities with their neutral molecules CHO and CHON. Both the CHO-related ions and CHON-related ions had higher concentrations during daytime than nighttime, which agrees with the variations of neutral CHO and CHON molecules. Additionally, the diurnal variations of organic molecules adducted with the same reagent ions, such as $CHO\text{-}NO_3^-$ and $CHON\text{-}NO_3^-$, had an obvious increase at approximately 17:00, while the concentrations of $CHO\text{-}HSO_4^-$ and $CHON\text{-}HSO_4^-$ did not. These variations were more likely to be affected by the variations of the reagent ions NO_3^- and HSO_4^-. Thus, for organic ion clusters, both the concentrations of neutral molecules and their corresponding reagent ions would affect their concentrations.

An exception in the diurnal variations was observed for NO_3^-. There seemed to be no relationship between its diurnal variation and those of NO_x or HNO_3. Instead, NO_3^- has an opposite diurnal variation with CS in urban Beijing. The concentration of NO_3^- was more complicated those of HSO_4^- and the organic ions, as the loss of NO_3^- includes molecular-ion reactions with numerous other neutral molecules. These neutral molecules correlate well with CS (Nie et al., 2022), and thus their influences cannot be separated. Interestingly, the fractions of NO_3^- in total ion clusters also tended to be relatively constant (15%±5%) (Fig. S12), which may be the result of a balance between ion-molecular production and loss.

Fig. 6 Diurnal concentrations of neutral molecules and ions

https://doi.org/10.5194/egusphere-2022-1108
Preprint. Discussion started: 2 November 2022

3.4 Quantification of the sources and sinks of representative air ions

We further show that the ionization of H_2SO_4 and $C_3H_4O_4$ by NO_3^- and condensational loss to particles were the main formation and loss pathways for HSO_4^- and $C_3H_3O_4^-$ respectively. HSO_4^- and $C_3H_3O_4^-$ were chosen as they are one of the most abundant negative ions in different atmospheric environments. As shown in Fig. 7, the simulated concentrations of both HSO_4^- and $C_3H_3O_4^-$ by Eqs.6-7 have a good consistency with the measured concentrations, indicating that the considered production and loss pathways can reproduce the real ion concentration in this urban atmosphere. That is, the ionization of H_2SO_4 and $C_3H_4O_4$ by NO_3^- is the main production pathway. For both HSO_4^- and $C_3H_3O_4^-$, the condensational loss was the main loss pathway, contributing to more than 70% of the total loss rate, which explains why CS is a driving factor for the concentration of cluster ions in urban Beijing. Ion-ion recombination process only accounted for 6% and 8% of the total loss rates for HSO_4^- and $C_3H_3O_4^-$, which was due to the low ion concentrations compared to the cleaner sites. Notably, the ion-molecular reactions between the ions with H_2SO_4 could contribute to 19% of the loss of both HSO_4^- and $C_3H_3O_4^-$. This indicates that the transformation of ions back to neutral molecules is also noteworthy.

Fig. 7 The measured and simulated HSO_4^- and $C_3H_3O_4^-$.

4 Conclusions

We quantified the composition-resolved ion concentrations in the atmosphere by combining mass spectrometry and electrical mobility measurements. The absolute transmission efficiency in the mass spectrometry APi-HTOF obtained with the ion mobility spectrometer agreed well with the relative transmission efficiency obtained in the chemical ionization mode of the APi-HTOF. The calibrated ion concentrations with different *m/z* ranges agreed well with the concentration of ions with corresponding mobility ranges of the ion mobility spectrometer. These indicate that an APi-HTOF can be well calibrated by running an APi-HTOF and an ion mobility spectrometer side by side in ambient measurements. Furthermore, we propose that the transmission efficiency of a CI-APi-TOF can also be obtained through *in-situ* comparison with an ion mobility spectrometer, as long as the X-ray and voltages of a chemical ionization inlet are turned off and atmospheric ions are directly measured.

The cluster ion composition and concentrations in urban Beijing are largely affected by the high concentration of large particles and nitrogen oxides. Firstly, ion concentration decreased significantly with an increasing CS for cluster ions in all the mobility ranges, as the ion loss rate increased. Median cluster ion concentrations in urban Beijing were only ~85 cm^{-3}, much lower than those reported at clean and rural sites due to the high CS in urban Beijing. Under similar levels of CS, the ion concentration of a specific compound was positively related to its neutral gas precursor and reagent ion concentrations. Due to high concentrations of nitrogen oxides in urban Beijing, the ion compositions were composed of more inorganic and organic nitrogen-containing species, with much higher fractions than those in Hyytiälä. This is

https://doi.org/10.5194/egusphere-2022-1108
Preprint. Discussion started: 2 November 2022

consistent with the higher neutral nitrogen-containing molecular fractions in urban Beijing as previously reported.

The negative organic cluster ions in urban Beijing were mostly oxygenated organic molecules that can be ionized by NO_3^- and HSO_4^-. NO_3^- and HSO_4^- were the most abundant ions in urban Beijing, and they also acted as the main reagent ions to generate air cluster ions. The formation pathway of HSO_4^- and $C_3H_3O_4^-$ were well characterized by the ionization of H_2SO_4 and $C_3H_4O_4$ by NO_3^-, and their loss processes were dominated by condensation loss, with minor contributions from ion-molecular reactions and ion-ion recombination. In all, the revealed governing factors of atmospheric cluster ion concentration and composition at polluted urban sites are useful in predicting ion concentrations and compositions, and can help evaluate air ion effects on human health, air quality, and global climate.

Data availability

Data and materials are available upon request to the corresponding authors.

Author contributions

RY and JK designed the study. RY, XL, CY, RC, YZ, JK, NS, and JL participated in data collection and performed the data analysis. RY and XL prepared the first version of the manuscript with contributions from all co-authors. All authors verified the final version of the manuscript.

Competing interests

The authors declare that they have no conflict of interest.

Acknowledgments

This research has been supported by National Natural Science Foundation of China (grant no. 22188102, 92044301, and 22106083), Samsung $PM_{2.5}$ SRP, the Academy of Finland (grant no. 337549, 302958, 337549, 1325656, 316114, 325647, and 332547), and European Research Council (grant no. 742206). The authors gratefully acknowledge the support of the research teams in AHL/BUCT laboratory and SMEAR II station.

https://doi.org/10.5194/egusphere-2022-1108
Preprint. Discussion started: 2 November 2022

References

Bates, D. R.: Recombination of Small Ions in the Troposphere and Lower Stratosphere, Planetary and Space Science, 30, 1275-1282, Doi 10.1016/0032-0633(82)90101-5, 1982.

Beck, L. J., Schobesberger, S., Sipilä, M., Kerminen, V. M., and Kulmala, M.: Estimation of sulfuric acid concentration using ambient ion composition and concentration data obtained with atmospheric pressure interface time-of-flight ion mass spectrometer, Atmos. Meas. Tech., 15, 1957-1965, 10.5194/amt-15-1957-2022, 2022.

Beig, G. and Brasseur, G. P.: Model of tropospheric ion composition: A first attempt, J. Geophys. Res.: Atmos., 105, 22671-22684, Doi 10.1029/2000jd900119, 2000.

Bertram, T. H., Kimmel, J. R., Crisp, T. A., Ryder, O. S., Yatavelli, R. L. N., Thornton, J. A., Cubison, M. J., Gonin, M., and Worsnop, D. R.: A field-deployable, chemical ionization time-of-flight mass spectrometer, Atmos. Meas. Tech., 4, 1471-1479, 10.5194/amt-4-1471-2011, 2011.

Bianchi, F., Garmash, O., He, X., Yan, C., Iyer, S., Rosendahl, I., Xu, Z., Rissanen, M. P., Riva, M., Taipale, R., Sarnela, N., Petäjä, T., Worsnop, D. R., Kulmala, M., Ehn, M., and Junninen, H.: The role of highly oxygenated molecules (HOMs) in determining the composition of ambient ions in the boreal forest, Atmos. Chem. Phys., 17, 13819-13831, 10.5194/acp-17-13819-2017, 2017.

Bianchi, F., Trostl, J., Junninen, H., Frege, C., Henne, S., Hoyle, C. R., Molteni, U., Herrmann, E., Adamov, A., Bukowiecki, N., Chen, X., Duplissy, J., Gysel, M., Hutterli, M., Kangasluoma, J., Kontkanen, J., Kurten, A., Manninen, H. E., Munch, S., Perakyla, O., Petaja, T., Rondo, L., Williamson, C., Weingartner, E., Curtius, J., Worsnop, D. R., Kulmala, M., Dommen, J., and Baltensperger, U.: New particle formation in the free troposphere: A question of chemistry and timing, Science, 352, 1109-1112, 10.1126/science.aad5456, 2016.

Cai, R. L., Yang, D. S., Fu, Y. Y., Wang, X., Li, X. X., Ma, Y., Hao, J. M., Zheng, J., and Jiang, J. K.: Aerosol surface area concentration: a governing factor in new particle formation in Beijing, Atmos. Chem. Phys., 17, 12327-12340, 10.5194/acp-17-12327-2017, 2017.

Carslaw, K. S., Harrison, R. G., and Kirkby, J.: Cosmic Rays, Clouds, and Climate, 298, 1732-1737, doi:10.1126/science.1076964, 2002.

Charlson, R. J., Schwartz, S. E., Hales, J. M., Cess, R. D., Coakley, J. A., Jr., Hansen, J. E., and Hofmann, D. J.: Climate forcing by anthropogenic aerosols, Science, 255, 423-430, 10.1126/science.255.5043.423, 1992.

Chen, X., Kerminen, V.-M., Paatero, J., Paasonen, P., Manninen, H. E., Nieminen, T., Petäjä, T., and Kulmala, M.: How do air ions reflect variations in ionising radiation in the lower atmosphere in a boreal forest?, Atmos. Chem. Phys., 16, 14297-14315, 10.5194/acp-16-14297-2016, 2016.

Chen, X., Virkkula, A., Kerminen, V.-M., Manninen, H. E., Busetto, M., Lanconelli, C., Lupi, A., Vitale, V., Del Guasta, M., Grigioni, P., Vaananen, R., Duplissy, E.-M., Petaja, T., and Kulmala, M.: Features in air ions measured by an air ion spectrometer (AIS) at Dome C, Atmos. Chem. Phys., 17, 13783-13800, 10.5194/acp-17-13783-2017, 2017.

Cheng, X., Chen, Q., Jie Li, Y., Zheng, Y., Liao, K., and Huang, G.: Highly oxygenated organic molecules produced by the oxidation of benzene and toluene in a wide range of OH exposure and NOx conditions, Atmos. Chem. Phys., 21, 12005–12019, 10.5194/acp-21-12005-2021, 2021.

https://doi.org/10.5194/egusphere-2022-1108
Preprint. Discussion started: 2 November 2022

513 Chu, C.-H., Chen, S.-R., Wu, C.-H., Cheng, Y.-C., Cho, Y.-M., and Chang, Y.-K.: The effects of negative air ions on cognitive
514 function: an event-related potential (ERP) study, International Journal of Biometeorology, 63, 1309-1317, 10.1007/s00484-
515 019-01745-7, 2019.

516 Curtius, J., Lovejoy, E. R., and Froyd, K. D.: Atmospheric ion-induced aerosol nucleation, Space Science Reviews, 125, 159-
517 167, 10.1007/s11214-006-9054-5, 2006.

518 Davidson, J. A., Fehsenfeld, F. C., and Howard, C. J.: The heats of formation of NO3− and NO3− association complexes with
519 HNO3 and HBr, 9, 17-29, https://doi.org/10.1002/kin.550090104, 1977.

520 Dos Santos, V. N., Herrmann, E., Manninen, H. E., Hussein, T., Hakala, J., Nieminen, T., Aalto, P. P., Merkel, M., Wiedensohler,
521 A., Kulmala, M., Petaja, T., and Hameri, K.: Variability of air ion concentrations in urban Paris, Atmos. Chem. Phys., 15,
522 13717-13737, 10.5194/acp-15-13717-2015, 2015.

523 Ehn, M., Junninen, H., Petaja, T., Kurten, T., Kerminen, V. M., Schobesberger, S., Manninen, H. E., Ortega, I. K., Vehkamaki,
524 H., Kulmala, M., and Worsnop, D. R.: Composition and temporal behavior of ambient ions in the boreal forest, Atmos. Chem.
525 Phys., 10, 8513-8530, 10.5194/acp-10-8513-2010, 2010.

526 Ehn, M., Junninen, H., Schobesberger, S., Manninen, H. E., Franchin, A., Sipila, M., Petaja, T., Kerminen, V. M., Tammet, H.,
527 Mirme, A., Mirme, S., Horrak, U., Kulmala, M., and Worsnop, D. R.: An Instrumental Comparison of Mobility and Mass
528 Measurements of Atmospheric Small Ions, Aerosol Sci. Technol., 45, 522-532, 10.1080/02786826.2010.547890, 2011.

529 Eisele, F. L.: Natural and Anthropogenic Negative-Ions in the Troposphere, J. Geophys. Res.: Atmos., 94, 2183-2196, DOI
530 10.1029/JD094iD02p02183, 1989.

531 Eisele, F. L. and Tanner, D. J.: Identification of Ions in Continental Air, J. Geophys. Res.: Atmos., 95, 20539-20550, DOI
532 10.1029/JD095iD12p20539, 1990.

533 Eisele, F. L. and Tanner, D. J.: Measurement of the gas phase concentration of H2SO4 and methane sulfonic acid and estimates
534 of H2SO4 production and loss in the atmosphere, J. Geophys. Res.: Atmos., 98, 9001-9010, https://doi.org/10.1029/93JD00031,
535 1993.

536 Eisele, F. L., Lovejoy, E. R., Kosciuch, E., Moore, K. F., Mauldin III, R. L., Smith, J. N., McMurry, P. H., and Iida, K.: Negative
537 atmospheric ions and their potential role in ion-induced nucleation, 111, https://doi.org/10.1029/2005JD006568, 2006.

538 Friedlander, S. K.: Smoke, dust, and haze, Oxford university press New York2000.

539 G. Baumgaertner, A. J., Thayer, J. P., Neely III, R. R., and Lucas, G.: Toward a comprehensive global electric circuit model:
540 Atmospheric conductivity and its variability in CESM1(WACCM) model simulations, 118, 9221-9232,
541 https://doi.org/10.1002/jgrd.50725, 2013.

542 Gautam, A. S., Siingh, D., and Kamra, A. K.: Statistical analysis of the atmospheric ion concentrations andmobility
543 distributions at a tropical station, Pune, Q J Roy Meteor Soc, 143, 2116-2128, 10.1002/qj.3071, 2017.

544 Gerdien and H.: Die absolute Messung der specifischen Leitfähigkeit und der Dichte des verticalen Leitungsstromes in der
545 Atmosphäre, J. Geophys. Res., 10, 65, 1903.

546 Gerdien, H.: Demonstration eines Apparates zur absoluten Messung der elektrischen Leitfahigkeit der Luft, Phys. Z., 6, 800-
547 801, 1905.

https://doi.org/10.5194/egusphere-2022-1108
Preprint. Discussion started: 2 November 2022

548 Harrison, R. G.: Ion-aerosol-cloud processes in the lower atmosphere, Reviews of Geophysics, 41, 1012,
549 10.1029/2002rg000114, 2003.

550 Heinritzi, M., Simon, M., Steiner, G., Wagner, A. C., Kürten, A., Hansel, A., and Curtius, J.: Characterization of the mass-
551 dependent transmission efficiency of a CIMS, Atmos. Meas. Tech., 9, 1449-1460, 10.5194/amt-9-1449-2016, 2016.

552 Hirsikko, A., Paatero, J., Hatakka, J., and Kulmala, M.: The 222Rn activity concentration, external radiation dose and air ion
553 production rates in a boreal forest in Finland between March 2000 and June 2006, 12, 265-278, 2007.

554 Hirsikko, A., Nieminen, T., Gagné, S., Lehtipalo, K., Manninen, H. E., Ehn, M., Hõrrak, U., Kerminen, V. M., Laakso, L.,
555 McMurry, P. H., Mirme, A., Mirme, S., Petäjä, T., Tammet, H., Vakkari, V., Vana, M., and Kulmala, M.: Atmospheric ions and
556 nucleation: a review of observations, Atmos. Chem. Phys., 11, 767-798, 10.5194/acp-11-767-2011, 2011.

557 Horrak, U., Salm, J., and Tammet, H.: Statistical characterization of air ion mobility spectra at Tahkuse Observatory:
558 Classification of air ions, J. Geophys. Res-Atmos., 105, 9291-9302, 10.1029/1999jd901197, 2000.

559 Iida, K., Stolzenburg, M., McMurry, P., Dunn, M. J., Smith, J. N., Eisele, F., and Keady, P.: Contribution of ion-induced
560 nucleation to new particle formation: Methodology and its application to atmospheric observations in Boulder, Colorado, J.
561 Geophys. Res.: Atmos., 111, https://doi.org/10.1029/2006JD007167, 2006.

562 Isidorov, V. A., Zenkevich, I. G., and Ioffe, B. V.: Volatile organic compounds in the atmosphere of forests, Atmospheric
563 Environment (1967), 19, 1-8, https://doi.org/10.1016/0004-6981(85)90131-3, 1985.

564 Jen, C. N., Hanson, D. R., and McMurry, P. H.: Toward Reconciling Measurements of Atmospherically Relevant Clusters by
565 Chemical Ionization Mass Spectrometry and Mobility Classification/Vapor Condensation, Aerosol Sci. Technol., 49, i-iii,
566 10.1080/02786826.2014.1002602, 2015.

567 Jiang, S.-Y., Ma, A., and Ramachandran, S.: Negative air ions and their effects on human health and air quality improvement,
568 International journal of molecular sciences, 19, 2966, 2018.

569 Jokinen, T., Sipilä, M., Junninen, H., Ehn, M., Lönn, G., Hakala, J., Petäjä, T., Mauldin, R. L., Kulmala, M., and Worsnop, D.
570 R.: Atmospheric sulphuric acid and neutral cluster measurements using CI-APi-TOF, Atmos. Chem. Phys., 12, 4117-4125,
571 10.5194/acp-12-4117-2012, 2012.

572 Junninen, H., Ehn, M., Petäjä, T., Luosujärvi, L., Kotiaho, T., Kostiainen, R., Rohner, U., Gonin, M., Fuhrer, K., Kulmala, M.,
573 and Worsnop, D. R.: A high-resolution mass spectrometer to measure atmospheric ion composition, Atmos. Meas. Tech., 3,
574 1039-1053, 10.5194/amt-3-1039-2010, 2010.

575 Kawamoto, H. and Ogawa, T.: A steady state model of negative ions in the lower stratosphere, Planetary and Space Science,
576 32, 1223-1233, https://doi.org/10.1016/0032-0633(84)90066-7, 1984.

577 Kirkby, J., Duplissy, J., Sengupta, K., Frege, C., Gordon, H., Williamson, C., Heinritzi, M., Simon, M., Yan, C., Almeida, J.,
578 Tröstl, J., Nieminen, T., Ortega, I. K., Wagner, R., Adamov, A., Amorim, A., Bernhammer, A.-K., Bianchi, F., Breitenlechner,
579 M., Brilke, S., Chen, X., Craven, J., Dias, A., Ehrhart, S., Flagan, R. C., Franchin, A., Fuchs, C., Guida, R., Hakala, J., Hoyle,
580 C. R., Jokinen, T., Junninen, H., Kangasluoma, J., Kim, J., Krapf, M., Kürten, A., Laaksonen, A., Lehtipalo, K., Makhmutov,
581 V., Mathot, S., Molteni, U., Onnela, A., Peräkylä, O., Piel, F., Petäjä, T., Praplan, A. P., Pringle, K., Rap, A., Richards, N. A.
582 D., Riipinen, I., Rissanen, M. P., Rondo, L., Sarnela, N., Schobesberger, S., Scott, C. E., Seinfeld, J. H., Sipilä, M., Steiner, G.,
583 Stozhkov, Y., Stratmann, F., Tomé, A., Virtanen, A., Vogel, A. L., Wagner, A. C., Wagner, P. E., Weingartner, E., Wimmer, D.,

https://doi.org/10.5194/egusphere-2022-1108
Preprint. Discussion started: 2 November 2022

584 Winkler, P. M., Ye, P., Zhang, X., Hansel, A., Dommen, J., Donahue, N. M., Worsnop, D. R., Baltensperger, U., Kulmala, M.,
585 Carslaw, K. S., and Curtius, J.: Ion-induced nucleation of pure biogenic particles, Nature, 533, 521-526, 10.1038/nature17953,
586 2016.

587 Kontkanen, J., Lehtinen, K. E. J., Nieminen, T., Manninen, H. E., Lehtipalo, K., Kerminen, V. M., and Kulmala, M.: Estimating
588 the contribution of ion–ion recombination to sub-2 nm cluster concentrations from atmospheric measurements, Atmos. Chem.
589 Phys., 13, 11391-11401, 10.5194/acp-13-11391-2013, 2013.

590 Krechmer, J. E., Groessl, M., Zhang, X., Junninen, H., Massoli, P., Lambe, A. T., Kimmel, J. R., Cubison, M. J., Graf, S., Lin,
591 Y.-H., Budisulistiorini, S. H., Zhang, H., Surratt, J. D., Knochenmuss, R., Jayne, J. T., Worsnop, D. R., Jimenez, J.-L., and
592 Canagaratna, M. R.: Ion mobility spectrometry–mass spectrometry (IMS–MS) for on- and offline analysis of atmospheric gas
593 and aerosol species, Atmos. Meas. Tech., 9, 3245-3262, 10.5194/amt-9-3245-2016, 2016.

594 Ku, B. K. and de la Mora, J. F.: Relation between Electrical Mobility, Mass, and Size for Nanodrops 1–6.5 nm in Diameter in
595 Air, Aerosol Sci. Technol., 43, 241-249, 10.1080/02786820802590510, 2009.

596 Kürten, A., Rondo, L., Ehrhart, S., and Curtius, J.: Calibration of a chemical ionization mass spectrometer for the measurement
597 of gaseous sulfuric acid, J. Phys. Chem. A, 116, 6375-6386, 10.1021/jp212123n, 2012.

598 Lee, B. U., Yermakov, M., and Grinshpun, S. A.: Removal of fine and ultrafine particles from indoor air environments by the
599 unipolar ion emission, Atmos. Environ., 38, 4815-4823, 10.1016/j.atmosenv.2004.06.010, 2004.

600 Lee, S.-H., Reeves, J. M., Wilson, J. C., Hunton, D. E., Viggiano, A. A., Miller, T. M., Ballenthin, J. O., and Lait, L. R.: Particle
601 formation by ion nucleation in the upper troposphere and lower stratosphere, Science, 301, 1886-1889,
602 doi:10.1126/science.1087236, 2003.

603 Lehtipalo, K., Yan, C., Dada, L., Bianchi, F., Xiao, M., Wagner, R., Stolzenburg, D., Ahonen, L. R., Amorim, A., Baccarini,
604 A., Bauer, P. S., Baumgartner, B., Bergen, A., Bernhammer, A. K., Breitenlechner, M., Brilke, S., Buchholz, A., Mazon, S. B.,
605 Chen, D. X., Chen, X. M., Dias, A., Dommen, J., Draper, D. C., Duplissy, J., Ehn, M., Finkenzeller, H., Fischer, L., Frege, C.,
606 Fuchs, C., Garmash, O., Gordon, H., Hakala, J., He, X. C., Heikkinen, L., Heinritzi, M., Helm, J. C., Hofbauer, V., Hoyle, C.
607 R., Jokinen, T., Kangasluoma, J., Kerminen, V. M., Kim, C., Kirkby, J., Kontkanen, J., Kurten, A., Lawler, M. J., Mai, H. J.,
608 Mathot, S., Mauldin, R. L., Molteni, U., Nichman, L., Nie, W., Nieminen, T., Ojdanic, A., Onnela, A., Passananti, M., Petaja,
609 T., Piel, F., Pospisilova, V., Quelever, L. L. J., Rissanen, M. P., Rose, C., Sarnela, N., Schallhart, S., Schuchmann, S., Sengupta,
610 K., Simon, M., Sipila, M., Tauber, C., Tome, A., Trostl, J., Vaisanen, O., Vogel, A. L., Volkamer, R., Wagner, A. C., Wang, M.
611 Y., Weitz, L., Wimmer, D., Ye, P. L., Ylisirnio, A., Zha, Q. Z., Carslaw, K. S., Curtius, J., Donahue, N. M., Flagan, R. C.,
612 Hansel, A., Riipinen, I., Virtanen, A., Winkler, P. M., Baltensperger, U., Kulmala, M., and Worsnop, D. R.: Multicomponent
613 new particle formation from sulfuric acid, ammonia, and biogenic vapors, Sci. Adv., 4, ARTN eaau5363

614 10.1126/sciadv.aau5363, 2018.

615 Li, X., Chee, S., Hao, J., Abbatt, J. P. D., Jiang, J., and Smith, J. N.: Relative humidity effect on the formation of highly oxidized
616 molecules and new particles during monoterpene oxidation, Atmos. Chem. Phys., 19, 1555-1570, 10.5194/acp-19-1555-2019,
617 2019.

618 Li, X., Li, Y., Lawler, M. J., Hao, J., Smith, J. N., and Jiang, J.: Composition of Ultrafine Particles in Urban Beijing:
619 Measurement Using a Thermal Desorption Chemical Ionization Mass Spectrometer, Environ. Sci. Technol., 55, 2859-2868,
620 10.1021/acs.est.0c06053, 2021.

https://doi.org/10.5194/egusphere-2022-1108
Preprint. Discussion started: 2 November 2022

Li, X., Li, Y., Cai, R., Yan, C., Qiao, X., Guo, Y., Deng, C., Yin, R., Chen, Y., Li, Y., Yao, L., Sarnela, N., Zhang, Y., Petäjä, T., Bianchi, F., Liu, Y., Kulmala, M., Hao, J., Smith, J. N., and Jiang, J.: Insufficient Condensable Organic Vapors Lead to Slow Growth of New Particles in an Urban Environment, Environ. Sci. Technol., 55, 9936-9946, 10.1021/acs.est.2c01566, 2022.

Liang, X., Zhou, Q., Wang, W., Wang, X., Chen, W., Chen, C., Li, Y., Hou, K., Li, J., and Li, H.: Sensitive detection of black powder by a stand-alone ion mobility spectrometer with an embedded titration region, Anal. Chem., 85, 4849-4852, 10.1021/ac400337s, 2013.

Ling, X., Jayaratne, R., and Morawska, L.: Air ion concentrations in various urban outdoor environments, Atmos. Environ., 44, 2186-2193, 10.1016/j.atmosenv.2010.03.026, 2010.

Liu, Y., Yan, C., Feng, Z., Zheng, F., Fan, X., Zhang, Y., Li, C., Zhou, Y., Lin, Z., Guo, Y., Zhang, Y., Ma, L., Zhou, W., Liu, Z., Dada, L., Daellenbach, K., Kontkanen, J., Cai, R., Chan, T., and Kulmala, M.: Continuous and comprehensive atmospheric observations in Beijing: a station to understand the complex urban atmospheric environment, Big Earth Data, 4, 295-321, 10.1080/20964471.2020.1798707, 2020.

Lovejoy, E. R.: Atmospheric ion-induced nucleation of sulfuric acid and water, J. Geophys. Res., 109, D08204, 10.1029/2003jd004460, 2004.

Lovejoy, E. R. and Curtius, J.: Cluster ion thermal decomposition (II): Master equation modeling in the low-pressure limit and fall-off regions. Bond energies for HSO4-(H2SO4)(x)(HNO3)(y), J. Phys. Chem. A, 105, 10874-10883, 10.1021/jp012496s, 2001.

Luts, A.: Evolution of negative small ions at enhanced ionization, J Geophys Res-Atmos, 100, 1487-1496, https://doi.org/10.1029/94JD01836, 1995.

Luts, A. and Salm, J.: Chemical-composition of small atmospheric ions near the ground, J Geophys Res-Atmos, 99, 10781-10785, Doi 10.1029/93jd03225, 1994.

Malcolm, C. P., Cowen, P. J., and Harmer, C. J.: Research Letter: High-density negative ion treatment increases positive affective memory, Psychological Medicine, 39, 1930-1932, 10.1017/S0033291709990444, 2009.

Manninen, H. E., Mirme, S., Mirme, A., Petaja, T., and Kulmala, M.: How to reliably detect molecular clusters and nucleation mode particles with Neutral cluster and Air Ion Spectrometer (NAIS), Atmos. Meas. Tech., 9, 3577-3605, 10.5194/amt-9-3577-2016, 2016.

Manninen, H. E., Petäjä, T., Asmi, E., Riipinen, I., Nieminen, T., Mikkilä, J., Hõrrak, U., Mirme, A., Mirme, S., and Laakso, L.: Long-term field measurements of charged and neutral clusters using Neutral cluster and Air Ion Spectrometer (NAIS), Boreal Environ. Res., 2009.

Mirme, A., Tamm, E., Mordas, G., Vana, M., Uin, J., Mirme, S., Bernotas, T., Laakso, L., Hirsikko, A., and Kulmala, M.: A wide-range multi-channel air ion spectrometer, Boreal. Environ. Res., 12, 247-264, 2007.

Mirme, S. and Mirme, A.: The mathematical principles and design of the NAIS - a spectrometer for the measurement of cluster ion and nanometer aerosol size distributions, Atmos. Meas. Tech., 6, 1061-1071, 10.5194/amt-6-1061-2013, 2013.

Möhler, O., Reiner, T., and Arnold, F.: The formation of SO_5^- by gas phase ion–molecule reactions, The Journal of Chemical Physics, 97, 8233-8239, 10.1063/1.463394, 1992.

https://doi.org/10.5194/egusphere-2022-1108
Preprint. Discussion started: 2 November 2022

656 Nie, W., Yan, C., Huang, D. D., Wang, Z., Liu, Y., Qiao, X., Guo, Y., Tian, L., Zheng, P., Xu, Z., Li, Y., Xu, Z., Qi, X., Sun, P.,
657 Wang, J., Zheng, F., Li, X., Yin, R., Dallenbach, K. R., Bianchi, F., Petäjä, T., Zhang, Y., Wang, M., Schervish, M., Wang, S.,
658 Qiao, L., Wang, Q., Zhou, M., Wang, H., Yu, C., Yao, D., Guo, H., Ye, P., Lee, S., Li, Y. J., Liu, Y., Chi, X., Kerminen, V.-M.,
659 Ehn, M., Donahue, N. M., Wang, T., Huang, C., Kulmala, M., Worsnop, D., Jiang, J., and Ding, A.: Secondary organic aerosol
660 formed by condensing anthropogenic vapours over China's megacities, Nature Geoscience, 15, 255-261, 10.1038/s41561-022-
661 00922-5, 2022.

662 Qiao, X., Yan, C., Li, X., Guo, Y., Yin, R., Deng, C., Li, C., Nie, W., Wang, M., Cai, R., Huang, D., Wang, Z., Yao, L., Worsnop,
663 D. R., Bianchi, F., Liu, Y., Donahue, N. M., Kulmala, M., and Jiang, J.: Contribution of Atmospheric Oxygenated Organic
664 Compounds to Particle Growth in an Urban Environment, Environ. Sci. Technol., 55, 13646–13656, 10.1021/acs.est.1c02095,
665 2021.

666 Riva, M., Rantala, P., Krechmer, J. E., Peräkylä, O., Zhang, Y., Heikkinen, L., Garmash, O., Yan, C., Kulmala, M., Worsnop,
667 D., and Ehn, M.: Evaluating the performance of five different chemical ionization techniques for detecting gaseous oxygenated
668 organic species, Atmos. Meas. Tech., 12, 2403-2421, 10.5194/amt-12-2403-2019, 2019.

669 Shuman, N. S., Hunton, D. E., and Viggiano, A. A.: Ambient and Modified Atmospheric Ion Chemistry: From Top to Bottom,
670 Chem. Rev., 115, 4542-4570, 10.1021/cr5003479, 2015.

671 Spangler, G. E. and Collins, C. I.: Reactant ions in negative ion plasma chromatography, Anal. Chem., 47, 393-402,
672 10.1021/ac60353a019, 1975.

673 Stano, M., Safonov, E., Kucera, M., and Matejcik, S.: Ion Mobility Spectrometry Study of Negative Corona Discharge in
674 Oxygen/Nitrogen Mixtures, Chem. Listy, 102, S1414-S1417, 2008.

675 Tammet, H.: Size and mobility of nanometer particles, clusters and ions, Journal of Aerosol Science, 26, 459-475,
676 https://doi.org/10.1016/0021-8502(94)00121-E, 1995.

677 Tammet, H.: Continuous scanning of the mobility and size distribution of charged clusters and nanometer particles in
678 atmospheric air and the Balanced Scanning Mobility Analyzer BSMA, Atmos. Res., 82, 523-535,
679 https://doi.org/10.1016/j.atmosres.2006.02.009, 2006.

680 Tammet, H.: Nanoion 2010-11, University of Tartu [dataset], http://dx.doi.org/10.15155/repo-2, 2015a.

681 Tammet, H., Hõrrak, U., Laakso, L., and Kulmala, M.: Factors of air ion balance in a coniferous forest according to
682 measurements in Hyytiälä, Finland, Atmos. Chem. Phys., 6, 3377-3390, 10.5194/acp-6-3377-2006, 2006.

683 Tammet, H. H., Urmas: FinEstIon2003_06. Dataset of air ion and atmospheric nanoparticle measurements, University of Tartu
684 [dataset], http://dx.doi.org/10.15155/repo-4, 2015b.

685 Tanner, D. J. and Eisele, F. L.: Ions in oceanic and continental air masses, J. Geophys. Res.: Atmos., 96, 1023-1031,
686 https://doi.org/10.1029/90JD02131, 1991.

687 Usoskin, I. G., Gladysheva, O. G., and Kovaltsov, G. A.: Cosmic ray-induced ionization in the atmosphere: spatial and temporal
688 changes, Journal of Atmospheric and Solar-Terrestrial Physics, 66, 1791-1796, https://doi.org/10.1016/j.jastp.2004.07.037,
689 2004.

690 Viggiano, A. A.: IN-SITU MASS-SPECTROMETRY AND ION CHEMISTRY IN THE STRATOSPHERE AND

https://doi.org/10.5194/egusphere-2022-1108
Preprint. Discussion started: 2 November 2022

691 TROPOSPHERE, Mass Spectrometry Reviews, 12, 115-137, 10.1002/mas.1280120203, 1993.

692 Viggiano, A. A., Perry, R. A., Albritton, D. L., Ferguson, E. E., and Fehsenfeld, F. C.: The role of H2SO4 in stratospheric
693 negative-ion chemistry, 85, 4551-4555, https://doi.org/10.1029/JC085iC08p04551, 1980.

694 Viggiano, A. A., Seeley, J. V., Mundis, P. L., Williamson, J. S., and Morris, R. A.: Rate constants for the reactions of XO_3^-
695 $(H_2O)_n$ (X = C, HC, and N) and $NO_3^-(HNO_3)_n$ with H_2SO_4: Implications for atmospheric detection of H_2SO_4, J. Phys. Chem.
696 A, 101, 8275-8278, DOI 10.1021/jp971768h, 1997.

697 Wiedensohler, A., Lütkemeier, E., Feldpausch, M., and Helsper, C.: Investigation of the bipolar charge distribution at various
698 gas conditions, Journal of aerosol science, 17, 413-416, 1986.

699 Wu, Z., Hu, M., Shao, K., and Slanina, J.: Acidic gases, NH3 and secondary inorganic ions in PM10 during summertime in
700 Beijing, China and their relation to air mass history, Chemosphere, 76, 1028-1035,
701 https://doi.org/10.1016/j.chemosphere.2009.04.066, 2009.

702 Yan, C., Dada, L., Rose, C., Jokinen, T., Nie, W., Schobesberger, S., Junninen, H., Lehtipalo, K., Sarnela, N., Makkonen, U.,
703 Garmash, O., Wang, Y., Zha, Q., Paasonen, P., Bianchi, F., Sipilä, M., Ehn, M., Petäjä, T., Kerminen, V.-M., Worsnop, D. R.,
704 and Kulmala, M.: The role of H2SO4-NH3 anion clusters in ion-induced aerosol nucleation mechanisms in the boreal forest,
705 Atmos. Chem. Phys., 18, 13231-13243, 10.5194/acp-18-13231-2018, 2018.

706 Yin, R., Yan, C., Cai, R., Li, X., Shen, J., Lu, Y., Schobesberger, S., Fu, Y., Deng, C., Wang, L., Liu, Y., Zheng, J., Xie, H.,
707 Bianchi, F., Worsnop, D. R., Kulmala, M., and Jiang, J.: Acid–Base Clusters during Atmospheric New Particle Formation in
708 Urban Beijing, Environ. Sci. Technol., 55, 10994-11005, 10.1021/acs.est.1c02701, 2021.

709 Zauner-Wieczorek, M., Curtius, J., and Kürten, A.: The ion–ion recombination coefficient α: comparison of temperature- and
710 pressure-dependent parameterisations for the troposphere and stratosphere, Atmos. Chem. Phys., 22, 12443-12465,
711 10.5194/acp-22-12443-2022, 2022.

712

https://doi.org/10.5194/egusphere-2022-1108
Preprint. Discussion started: 2 November 2022

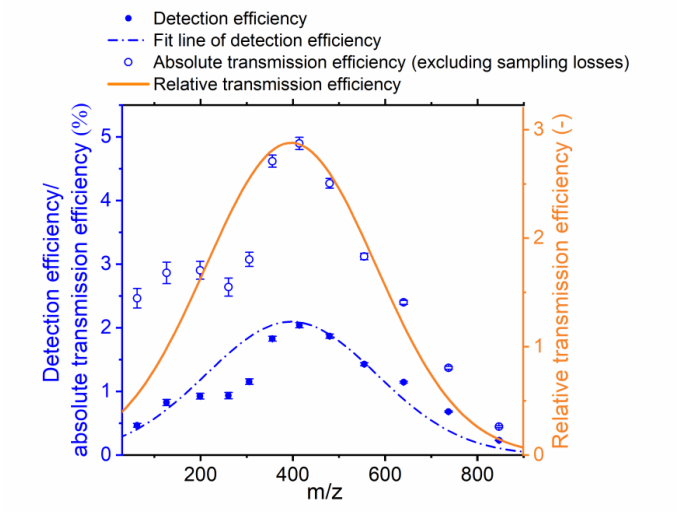

713

714 **Figure 1.** The detection efficiency and absolute transmission efficiency of APi-HTOF determined through the *in-situ*
715 comparison with NAIS and the relative transmission efficiency of APi-HTOF determined through the depletion method.
716 The relative transmission efficiency is obtained by dividing the detection efficiency by the sampling efficiency of cluster
717 ions. The voltage settings of APi-HTOF remain the same during the experiment.
718

https://doi.org/10.5194/egusphere-2022-1108
Preprint. Discussion started: 2 November 2022

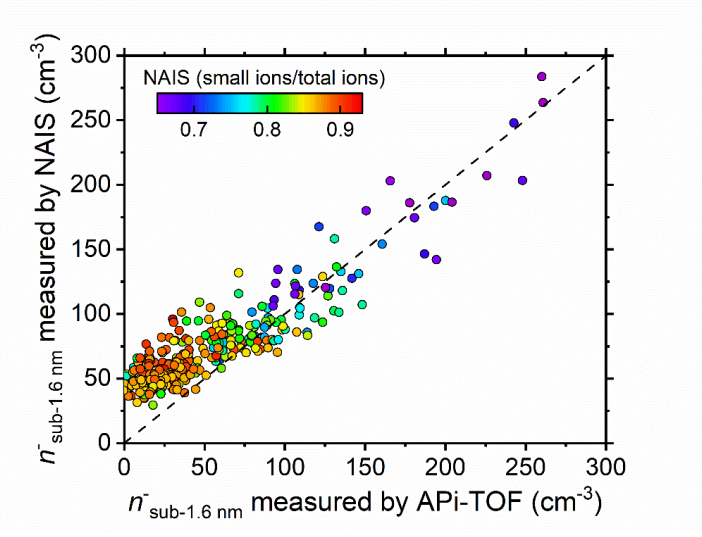

719

720 **Figure 2.** The total concentration of negative cluster ions ($n^-_{sub\text{-}1.6\ nm}$) measured by APi-HTOF is well correlated with
721 that measured by NAIS. Colors represent the ratio of negative ions smaller than 1.3 nm ($n^-_{sub\text{-}1.3\ nm}$) to negative cluster
722 ions ($n^-_{sub\text{-}1.6\ nm}$).

723

https://doi.org/10.5194/egusphere-2022-1108
Preprint. Discussion started: 2 November 2022

724

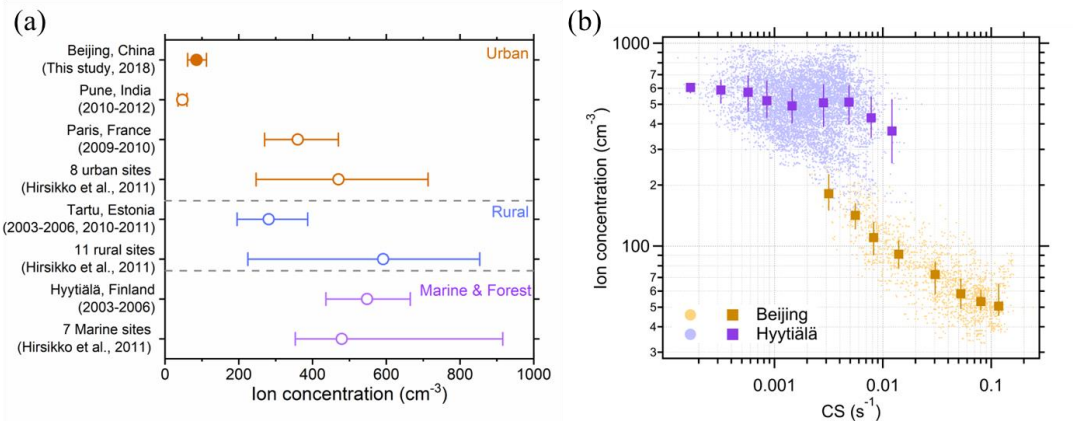

725

726 **Figure 3.** (a) Negative cluster ions observed in global urban, rural, forest, and marine sites. The circles represent the
727 median values, and the error bars represent the 25%-75% ranges. Ion mobility ranges for different sites were between sub-
728 1.6 and sub-2 nm. (b) The decreasing trends of the negative cluster ion concentrations with the increase of CS were
729 observed in both Beijing and Hyytiälä. The markers and error bars are median values and 25%-75% ranges, respectively.
730 For comparison, NAIS data were used for both urban Beijing and the clean forest site Hyytiälä.
731

https://doi.org/10.5194/egusphere-2022-1108
Preprint. Discussion started: 2 November 2022

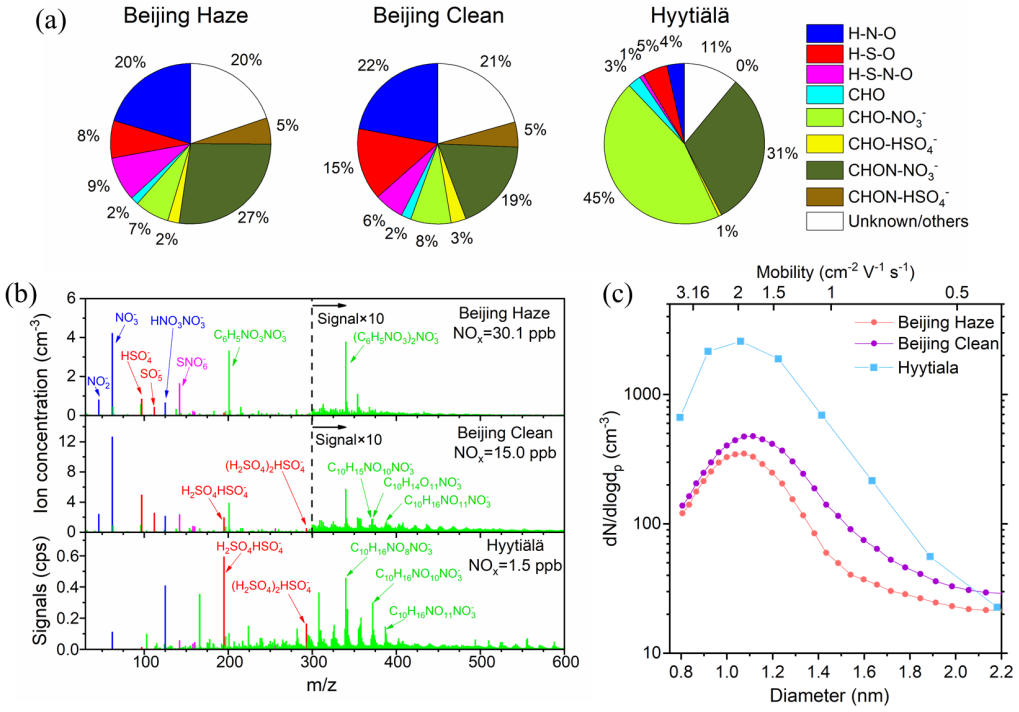

Figure 4. The chemical composition and size distributions of negative cluster ions observed in Beijing and Hyytiälä. (a) The species distributions of negative cluster ions during haze and clean periods in Beijing and Hyytiälä. (b) The average mass spectrums of negative cluster ions during clean and haze periods in Beijing and Hyytiälä measured by APi-HTOF. Signals for *m/z*>300 were multiplied by 10 times in Beijing for clearer views. Haze periods were identified based on whether $PM_{2.5}$ concentration is higher than 75 $\mu g \cdot m^{-3}$. The average NO_x concentrations for the three situations are 30.1, 15.0, and 1.5 ppb, respectively. (c) The ion mobility distributions and size distributions measured by NAIS.

https://doi.org/10.5194/egusphere-2022-1108
Preprint. Discussion started: 2 November 2022

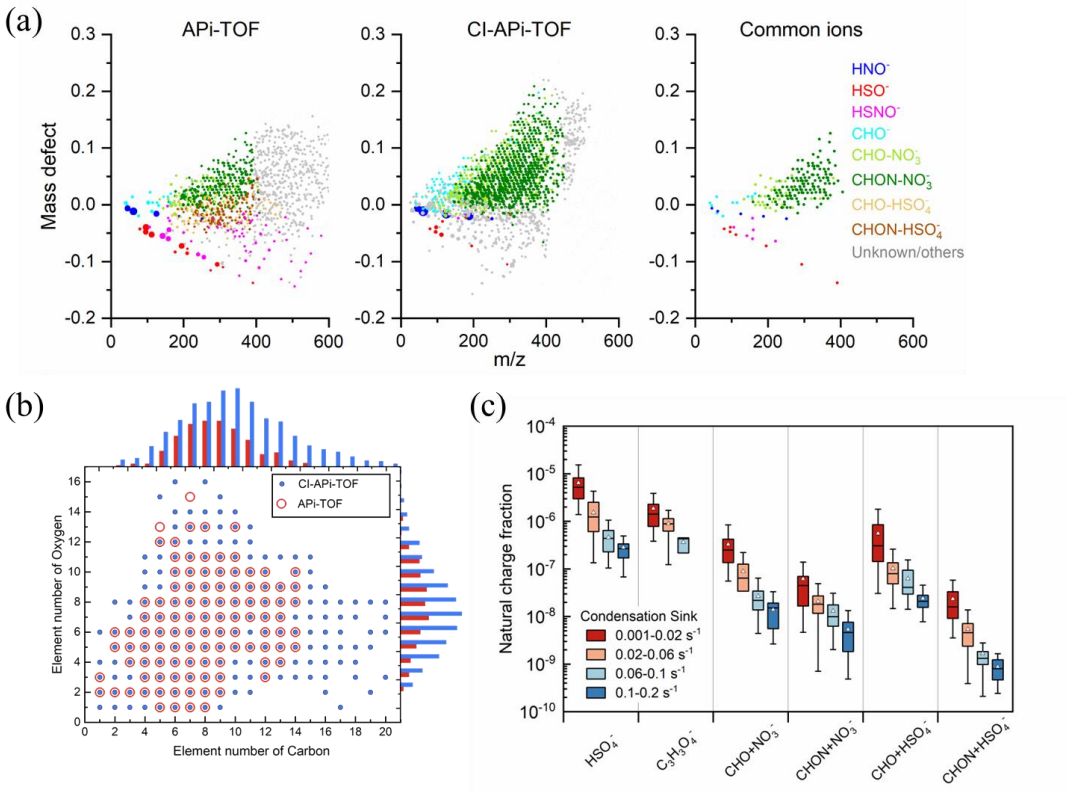

Figure 5. (a) The mass defect plots of the species detected in ions (APi-HTOF), neutral gases (CI-APi-LTOF), and their common species in urban Beijing; (b) Comparison of the species distribution of CHO and CHON organic ions and neutral gases with the number of C and O atoms. The N atom distributions were shown in Fig.S6. (c) The naturally charge ratios of HSO_4^-, $C_3H_3O_4^-$, $CHO\text{-}NO_3^-$, and $CHON\text{-}NO_3^-$. The ratios are calculated based on the concentration of specific ions and their corresponding neutral gases.

https://doi.org/10.5194/egusphere-2022-1108
Preprint. Discussion started: 2 November 2022

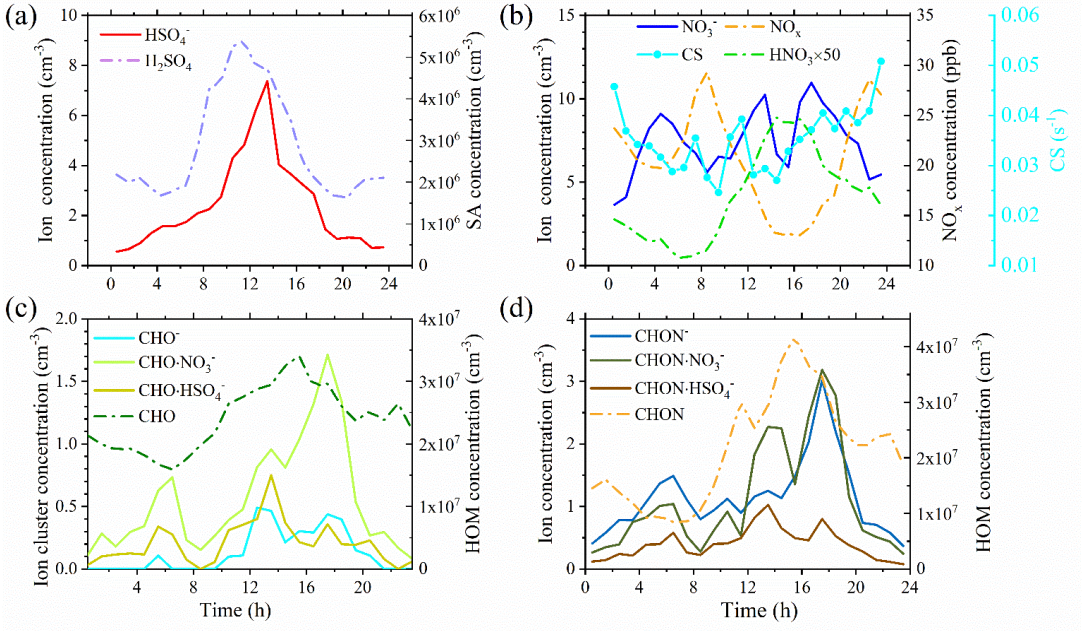

748

749 **Figure 6.** The diurnal variations of 8 types of ions measured by APi-HTOF and their corresponding neutral gases
750 measured by (nitrate-) CI-APi-LTOF. (a) HSO_4^- and H_2SO_4; (b) NO_3^-, NO_x, HNO_3, and CS; As HNO_3 was not
751 simultaneously measured with clusters ions, its diurnal variation is calculated from the measured results of another period,
752 from August 8th to October 23rd, 2019, and is consistent with that reported in a previous study (Wu et al., 2009); (c)
753 CHO^-, $CHO\text{-}NO_3^-$, $CHO\text{-}HSO_4^-$, and neutral CHO molecules; (d) $CHON^-$, $CHON\text{-}NO_3^-$, $CHON\text{-}HSO_4^-$, and neutral
754 CHON molecules.

755

https://doi.org/10.5194/egusphere-2022-1108
Preprint. Discussion started: 2 November 2022

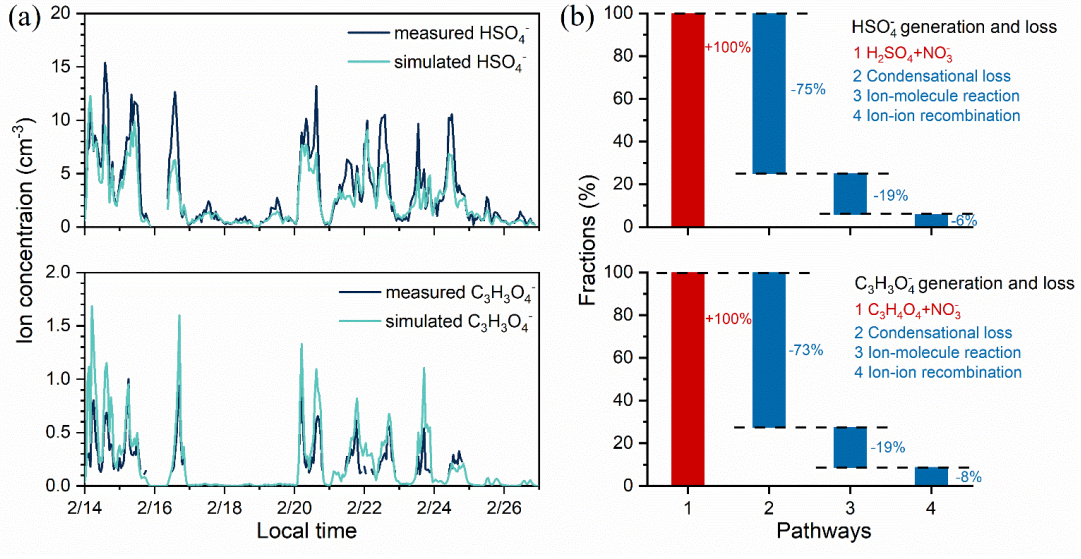

Figure 7. (a) The measured and simulated concentrations of HSO_4^- and $C_3H_3O_4^-$ in Beijing. The simulation is performed according to dynamic models as described in Section 2.3 and four formation and loss pathways were considered. (b) The fractions of the formation or loss rates of HSO_4^- and $C_3H_3O_4^-$ contributed by different pathways. The average values of the results were shown here.